2015 IEEE International Conference on Robotics and Automation (ICRA)
Washington State Convention Center
Seattle, Washington, May 26-30, 2015

Dual Quaternion Based Modal Kinematics for Multisection Continuum Arms

Isuru S. Godage# and Ian D. Walker*

Abstract— **This paper presents general modal dual Quaternion (DQ) kinematics for multisection continuum arms. DQ's produce higher accuracy than homogeneous transformation matrices (HTM) when transformed to modal shape functions (MSF) of similar order and are numerically stable. Thus, the model is compact, more accurate and computationally efficient than the modal kinematics proposed by the author based on HTM's. Also, DQ kinematics does not suffer from singularity related limitations of Euler angle based inverse orientation kinematics. Recursive schemes for deriving DQ's and DQ Jacobians are also presented and can be extended arbitrarily. Both modal HTM and modal DQ kinematics are then applied to solve illustrative spatial inverse position and orientation tracking problems. Based on the results, this paper quantitatively compares both methods and highlights the advantages of modal DQ kinematics. The proposed DQ kinematics are easily extensible to variable length multisection continuum arm with general actuator configurations.**

I. Introduction

Many continuum robotic arms have been designed and implemented for various applications over the years and have successfully proved their versatility in field deployments [1]. Continuum arms take inspiration from biological entities such as the musculature of tongues [2], cephalopod arms [3], [4], vine tentacles [5] etc. Many "true" continuum arms, as classified in [6], utilize elastic i.e., pneumatic muscle actuators [7] or backbone bending deformation [8] to generate motion. Consequently, contrary to rigid robots, all soft continuum robots have a much greater number of theoretical degrees of freedom (DoF) due to smooth bending along their structure. However, these mechanical deformations considerably increase the modeling complexity.

A multisection continuum arm is essentially a parallel-serial robot. Each continuum section is typically realized as a three-actuator parallel mechanism which is the optimal actuator configuration for spatial operation. However other actuator arrangements are possible [9]. The actuators are rigidly mounted at each end and constrained to actuate parallel to the continuum section. Upon actuation continuum sections deform in circular arc shapes. Kinematics through lumped approximation methods [10], [11], [12] denote the natural transition from rigid-linked to continuum arm modeling. But the large number of virtual rigid-link segments required to sufficiently emulate smooth bending significantly increase the overall DoF. This poses computational difficulties for extending to multisection continuum arms, in particular for inverse kinematics (IK) through iterative methods. Parametric kinematics avoid these complexities by defining kinematics with shape functions to accommodate continuous and smooth bending [13].

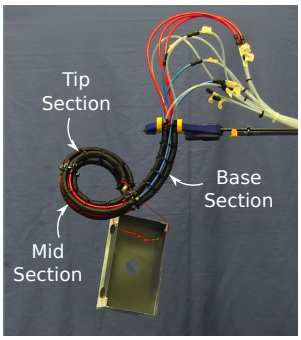

Fig. 1: Pneumatic muscle actuated state of the art multisection continuum arms. (a) Three-section continuum robotic arm prototype developed in the Italian Institute of Technology, Genova, Italy.

The parametric modal shape functions (MSF) for "hyper-redundant" robotic structures was proposed in [13]. It simplified kinematic analysis but limited corresponding robots to "application specific" and "reduced" set of shapes and motions. The curve parametric (CP) kinematics for multisection continuum arms proposed in [14] takes a modular approach to yield correct and structurally accurate results.Contrary to lumped models, CP kinematics are derived in true actuator variables, computationally efficient, and provides better physical interpretation. However CP kinematics cannot model straight (or near-straight) arm poses, i.e., when actuator lengths are equal (or near equal), due to an inherent numerical singularity.

The modal kinematics proposed in [15] was based on the CP principles but replaced the parametric terms with multivariate polynomial MSF's of joint space variables. The model demonstrated kinematic decoupling and spatial 6 DoF (position and orientation) trajectory tracking for various applications such as path planning [4]. Because the kinematics is derived in homogeneous transformation matrix (HTM) representation and uses Euler angles to calculate inverse orientation, it suffers from orientation related numerical problems when solving for certain IK. The Euler angle representation has several numerical limitations. It suffers from singularities as angles are discontinued at specific ranges as other angles go through the singularity [16]. Hence

Isuru S. Godage (corresponding author) is with the Department of Mechanical Engineering, Vanderbilt University, Nashville, TN 37212, USA. isuru.godage@vanderbilt.edu.

∗ Ian D. Walker is with the Department of Electrical and Computer Engineering, Clemson University, Clemson SC 29631, USA. iwalker@clemson.edu.

This work was supported in part by U.S. National Science Foundation Grant IIS-0904116 and part by NASA under contract NNX12AM01G.

these is the need for a better kinematics for hyper-redundant continuum arms that does not suffer from inverse orientation related numerical problems.

The dual Quaternion (DQ) representation does not suffer from these limitations [17]. Dual Quaternion is an ordered pair of Quaternions, one for orientation and one for position. DQ representation is unambiguous, accurate, and computationally efficient. Much like HTM, DQ can represent spatial (rotational and translational) transformations without compromise making it appealing for the task at hand. In addition to these advantages, it uses only 8 parameters (compare with HTM that uses 12) to define the complete spatial location thus requires less memory and computations. Because of the iterative IK solution process associated with multisection continuum arms due to high-redundancy this translate to significant computational time improvements.

This paper proposes DQ-based modal kinematics for multisection continuum arms to improve their accuracy and performance, particularly for IK. The organization of the paper is as follows. Section II first reviews the existing HTM modal kinematics and then presents the approach to derive modal DQ's for a continuum arm section of three-actuator configuration. The single section DQ representation is then extended and recursively implemented for an arbitrarily long multisection continuum arm in Section III. The performance and accuracy comparison is carried out in Section IV. Conclusions are presented in Section V.

II. Methodology

In this section, a review of state of the art modal kinematics is first summarized. Then the derivation of modal DQ for continuum sections and application to multisection continuum arms is detailed followed by an account of accuracy and performance. The mathematical operators utilized here onward are annotated in Table I.

A. Revisiting Modal Kinematics for Continuum Arms

Figure 2 shows the schematic of any i^{th} continuum section of a multisection continuum arm. It has three variable length actuators mounted at apexes of an equilateral triangle of sides $\sqrt{3}r_i$ where $r_i \in \mathbb{R}^+$ is the radius. Each actuator length at any time is given by $L_{i0} + l_{ij}$ where $l_{ij} \in \mathbb{R}$ the length change of the j^{th} actuator $(j \in \{1,2,3\})$ and$L_{i0} \in \mathbb{R}^+$ is the unactuated length of the section. Upon actuation the section deforms in a circular arc [14] of varying curvature characterized by three parameters; radius of curvature $\lambda_i \in (0,\infty)$ with instantaneous center C_i, angle subtended by

TABLE I: Mathematical Operators

Operator	Definition
$\odot$	Dual quaternion multiplication
$\circ$	Quaternion multiplication
$(\ )^*$	Quaternion conjugate
$\nabla_q(\ )$	Partial derivative with respect to vector $\boldsymbol{q}$.
$(\ )_{,x}$	Partial derivative with respect to variable $q_x \in \mathbb{R}$.
$(\ )^x$	x^{th} column vector of the enclosed matrix
$(\ )^\vee$	Form the vector from a angular velocity matrix.
$(\ )^\wedge$	Form the matrix from the angular velocity vector.

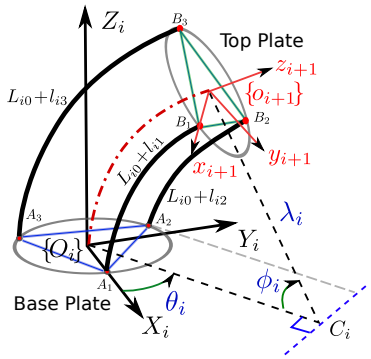

Fig. 2: Schematic of any i^{th} continuum section showing base $\{O_i\}$ and tip $\{O_{i+1}\}$ coordinate frames, curve parameters and actuator variables. All the calculations are carried out with respect to $\{O_i\}$.

the bending arc $\phi_i \in [0, 2\pi_{max}]$, and angle of the bending plane with respect to the $+X_i$, $\theta_i \in [-\pi, \pi]$. Utilizing these parameters, the CP HTM of the continuum section, ${}^c\mathbf{T} \in \mathtt{SE}(3)$ is given by [15]

$$
\begin{aligned}
{}^c\mathbf{T}_i(\xi_i, \boldsymbol{q}_i) &= \mathbf{R}_z(\theta_i)\mathbf{P}_x(\lambda_i)\mathbf{R}_y(\xi_i\phi_i)\mathbf{P}_x(-\lambda_i)\mathbf{R}_z^T(\theta_i) \\
&= \begin{bmatrix} {}^c\mathbf{R}_i(\xi_i, \boldsymbol{q}_i) & {}^c\boldsymbol{p}_i(\xi_i, \boldsymbol{q}_i) \\ \mathbf{0} & 1 \end{bmatrix} \qquad (1)
\end{aligned}
$$

where $\mathbf{R}_z$, $\mathbf{R}_y$ are rotational matrices about the $\boldsymbol{Z}$ and $\boldsymbol{Y}$ axes. $\mathbf{P}_x$ is the translation matrix along the $\boldsymbol{X}$ axis, $\boldsymbol{q}_i = [l_{i1}, l_{i2}, l_{i3}] \in \mathbb{R}^3$ is the joint space vector, ${}^c\mathbf{R}_i \in \mathtt{SO}(3)$ and ${}^c\boldsymbol{p}_i \in \mathbb{R}^3$ are respectively the CP rotational and translational matrices, and $\xi_i \in [0,1]$ defines the points along the neutral axis with $\xi_i = 0$ is the section base and $\xi_i = 1$ is the tip.

However, due to the dependency of the circular arc radius [15], λ, (or curvature, κ, in [14]) which approaches ∞ for straight/near-straight arm poses. This in turn introduce errors in the kinematic model within singularity neighborhoods. Figure 3 shows the error of $[{}^c\mathbf{T}]_{24}$ within $\boldsymbol{q} \to 0.03$ neighborhood. The modal kinematics for continuum arms proposed in [15] replace these numerically ill-defined CP HTM element terms with intuitive, structurally accurate, unique, and numerically stable multivariate polynomials of joint-space variables derived through Taylor series expansion. Further, no intermediary morphological transformations are required to map particular curve shapes and the approach thence avoids redefining application specific MSF's. The modal HTM derived from (1), $\mathbf{T}_i \in \mathtt{SE}(3)$, is given by

$$
\mathbf{T}_i(\xi_i, \boldsymbol{q}_i) = \begin{bmatrix} \mathbf{R}_i(\xi_i, \boldsymbol{q}_i) & \boldsymbol{p}_i(\xi_i, \boldsymbol{q}_i) \\ \mathbf{0} & 1 \end{bmatrix} \qquad (2)
$$

where $\mathbf{R}_i \in \mathtt{SO}(3)$ and $\boldsymbol{p}_i \in \mathbb{R}^3$ are respectively the modal rotation matrix and modal position vector along the neutral axis.

The modal HTM for a single continuum section given by (2) is extended to derive the forward kinematics of multisection continuum arms. Referring to Fig. 4, continuum sections are numbered incrementally from 1 (base section coinciding with the task coordinate frame $\{O\}$). Employing basic coordinate transformations, the modal HTM of the

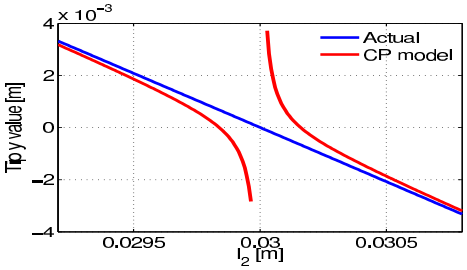

Fig. 3: Error of $[\mathbf{T}_c]_{24}$ for $l_{i2} \to 0.03$ where $l_{i1} = l_{i3} = 0.03$. The error spans within a singularity neighborhood thus eliminating the possibility of conditional HTM's such as [18] to counter the numerical instabilities.

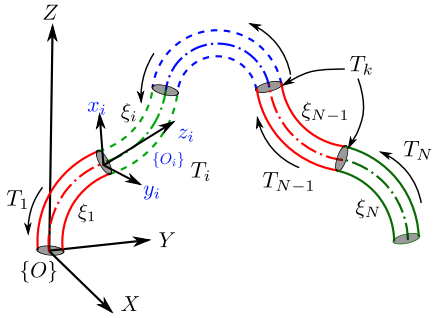

Fig. 4: Schematic of a general multisection continuum arm with N continuum sections.

neutral axis for any i^{th} continuum section relative to $\{O\}$, $\mathbf{T}^i \in \mathtt{SE}(3)$, is given by

$$\mathbf{T}^i(\xi_i, \boldsymbol{q}^i) = \prod_{k=1}^{i} \mathbf{T}_k(\xi_k, \boldsymbol{q}_k) = \begin{bmatrix} \Theta_i(\xi_i, \boldsymbol{q}^i) & \Psi_i(\xi_i, \boldsymbol{q}^i) \\ \mathbf{0} & 1 \end{bmatrix} \quad (3)$$

where $\boldsymbol{q}^i = [\boldsymbol{q}_1, \boldsymbol{q}_2, \cdots, \boldsymbol{q}_i]^T \in \mathbb{R}^{3i}$ is the actuated joint-space vector, $\Theta_i \in \mathtt{SO}(3)$ is the modal rotational matrix, $\Psi_i \in \mathbb{R}^3$ is the modal translation vector [15]. Note that the position and orientation of any i^{th} continuum section depends only on the preceding $(i-1)$ sections and is independent of the successive sections. To denote this, $\xi_k = 1, \forall k < i$ and $\xi_k = 0, \forall k > i$.

Because of the high redundancy, closed-form analytical inverse kinematics of multisection continuum arms are computationally infeasible. Hence multivariate iterative Newton-Raphson or constrained optimization algorithms are utilized to solve IK problems [19].

B. Modal Dual Quaternions for Continuum Sections

Dual Quaternion is an ordered pairs of Quaternions composed by applying Clifford dual number algebra on Quaternions. Let $\boldsymbol{Q}_i = (\boldsymbol{s}_i + \epsilon \boldsymbol{t}_i) \in \mathbb{R}^8$ be the DQ corresponds to the i^{th} continuum section where $\boldsymbol{s}_i \in \mathbb{R}^4$ is the rotational Quaternion, $\boldsymbol{t}_i \in \mathbb{R}^4$ is the translational Quaternion. The dual operator ϵ is defined as $\epsilon^2 = 0$ and $\epsilon \neq 0$. Analogous to complex number representations, ϵ distinguishes the rotational and translational components. Note that, this paper lists rotational Quaternions first in the DQ notation.

There exists a unique mapping between HTM's and DQ's [20]. Let ${}^c\boldsymbol{Q}_i$ be the curve parametric DQ of the i^{th}continuum section. Hence ${}^c\boldsymbol{Q}_i$ can be derived from the CP HTM. First, the rotational matrix, ${}^c\mathbf{R}_i$, derived in (1) is transformed to unit rotational Quaternion, ${}^c\boldsymbol{s}_i = \langle {}^cs_i^x, {}^cs_i^y, {}^cs_i^z, {}^cs_i^0 \rangle$ where ${}^cs_i^0 \in \mathbb{R}$ is the scalar rotation angle and $\langle {}^cs_i^x, {}^cs_i^y, {}^cs_i^z \rangle \in \mathbb{R}^3$ is the angle axis vector, as follows[1].

$$\begin{aligned} {}^cs_i^0(\xi_i, \boldsymbol{q}_i) &= \tfrac{1}{2}\sqrt{[{}^c\mathbf{R}_i]_{11} + [{}^c\mathbf{R}_i]_{22} + [{}^c\mathbf{R}_i]_{33} + 1} \\ {}^cs_i^x(\xi_i, \boldsymbol{q}_i) &= \tfrac{1}{4\,{}^cs_i^0}\left([{}^c\mathbf{R}_i]_{32} - [{}^c\mathbf{R}_i]_{23}\right) \\ {}^cs_i^y(\xi_i, \boldsymbol{q}_i) &= \tfrac{1}{4\,{}^cs_i^0}\left([{}^c\mathbf{R}_i]_{13} - [{}^c\mathbf{R}_i]_{31}\right) \\ {}^cs_i^z(\xi_i, \boldsymbol{q}_i) &= \tfrac{1}{4\,{}^cs_i^0}\left([{}^c\mathbf{R}_i]_{21} - [{}^c\mathbf{R}_i]_{12}\right) \end{aligned} \quad (4)$$

Utilizing ${}^c\boldsymbol{s}_i$, the translational component, ${}^c\boldsymbol{t}_i = \langle {}^ct_i^v, {}^ct_i^0 \rangle$ is then derived as

$${}^c\boldsymbol{t}_i(\xi_i, \boldsymbol{q}_i) = \tfrac{1}{2}\langle {}^c\boldsymbol{p}_i, 0\rangle \circ {}^c\boldsymbol{s}_i \quad (5)$$

where ${}^ct_i^v$ is the vector portion of the Quaternion and ${}^c\boldsymbol{p}_i$ is converted to $\mathbb{R}^4$ space by appending a trailing zero. The Quaternion multiplication is defined by $\langle \boldsymbol{a}_v, a_0\rangle \circ \langle \boldsymbol{b}_v, b_0\rangle = \langle a_0\boldsymbol{b}_v + b_0\boldsymbol{a}_v + \boldsymbol{a}_v \times \boldsymbol{b}_v, a_0b_0 - \boldsymbol{a}_v \cdot \boldsymbol{b}_v\rangle$.

The CP DQ derivation of any i^{th} continuum section is now completed. Note that the DQ for a general continuum section, given by (4) and (5)) can be utilized for any continuum section (with varying mechanical parameters such as L_0 and r) simply by substituting these values in the computation of curve parameters (λ_i, ϕ_i and θ_i listed in [15]). Because of the numerical instabilities associated with the CP kinematics, as detailed in [15], [21], both (4) and (5) suffer from the same numerical problems found in (1) yielding undefined and incorrect solutions within singular neighborhoods. To circumvent these problems, we derive MSF's for each DQ element derived in (4) and (5) as described in [15]. Let the modal DQ derived from ${}^c\boldsymbol{Q}_i$ be ${}^c\boldsymbol{Q}_i = (\boldsymbol{s}_i + \epsilon \boldsymbol{t}_i)$. The resulting multivariate polynomial MSF's are defined for all values within their actuation range without the need of specific singularity resolving techniques such as those proposed in [18].

C. Accuracy and Performance Comparison

The MSF approach detailed in [15] is a high dimensional approximation technique but is straightforward and readily derived by means of modern computer algebra systems. Accuracy is a critical metric in engineering approximation methods. We next compare the accuracy of modal HTM and DQ systems. First, the position and orientation error metrics, denoted e_p and e_R respectively, employed in this paper is defined as [22]

$$e_p = \|\boldsymbol{p}_c - \boldsymbol{p}^*\| \quad (6)$$

$$e_R = \tfrac{1}{2}\textstyle\sum_{k=1}^{3} \|(\mathbf{R}_c)_k \times (\mathbf{R}^*)_k\| \quad (7)$$

where $\boldsymbol{p}^*$ and $\mathbf{R}^*$ are substituted with modal position and orientation matrices computed with modal HTM and DQ representations. The cross product is denoted with $\times$ and $(\,)_k$ are the orthonormal orientation vectors of enclosed rotation matrices.

The maximum bending angle (ϕ_{max}) of the prototype continuum section shown in Fig. 1 is close to 184°(when

[1]Note that there are varying ways to compute the Quaternion from the rotational matrix to avoid numerical scaling problems. But for ease of presentation, only this method is presented.

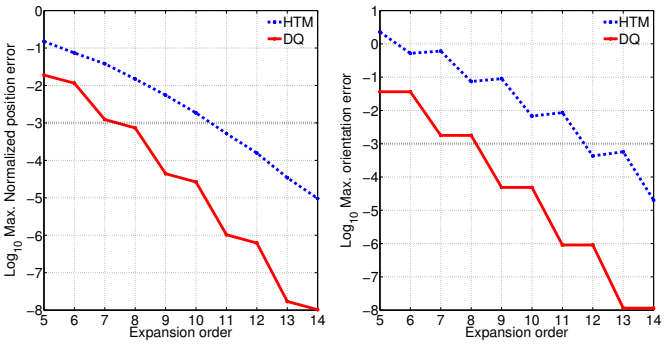

(a) (b)

Fig. 5: Error comparison between the modal HTM and modal DQ against the approximation expansion order (a) position error from (6) normalized to the original section length $L_{i0} = 0.15m$, (b) maximum orientation error from (7). The reference lines denote 0.001.

$l_{i1} = 0$ and $l_{i2} = l_{i3} = 0.06m$). At ϕ_{max}, normalized (to the original length of actuators, L_{i0}) maximum position error (e_p) variation for both modal HTM and DQ systems are plotted against the Taylor series expansion order in Fig. 5a. Similarly, orientation error (e_R) variation is plotted against the expansion order in Fig. 5b. It is observed that for attaining a given accuracy, the DQ representation requires an expansion 2-3 orders less. This order reduction is proportional to ϕ_{max} and results in fewer terms in MSF's. This corresponds to significant computational time and memory usage improvement, particularly for multisection continuum arm calculations as will be illustrated in the next section.

III. Dual Quaternion Recursive Kinematics for Multisection Continuum Arms

Akin to HTM based kinematics, coordinate transformation is defined for DQ systems. If $\{\boldsymbol{O}_i\}$ and $\{\boldsymbol{O}_j\}$ are two reference frames with respect to a fixed frame of reference, $\{O\}$, while $\boldsymbol{Q}_i$ and $\boldsymbol{Q}_j$ are the DQ's of those reference frames relative to $\{O\}$, then spatial coordinate transformation from $\{\boldsymbol{O}_i\}$ to $\{\boldsymbol{O}_j\}$ is denoted by

$$\boldsymbol{Q}_i \odot \boldsymbol{Q}_j = \boldsymbol{s}_i \circ \boldsymbol{s}_j + \epsilon\left(\boldsymbol{s}_i \circ \boldsymbol{t}_j + \boldsymbol{t}_i \circ \boldsymbol{s}_j\right) \tag{8}$$

Hence, analogous to (3), the complete DQ forward kinematics of any i^{th} continuum section relative to $\{O\}$, denoted by $\boldsymbol{Q}^i$, is given by

$$\begin{aligned}\boldsymbol{Q}^i\left(\xi_i, \boldsymbol{q}^i\right) &= \boldsymbol{Q}_1 \odot \boldsymbol{Q}_2 \odot \cdots \odot \boldsymbol{Q}_i \\ &= \boldsymbol{u}_i\left(\xi_i, \boldsymbol{q}^i\right) + \epsilon \boldsymbol{v}_i\left(\xi_i, \boldsymbol{q}^i\right)\end{aligned} \tag{9}$$

where $\boldsymbol{u}_i \in \mathbb{R}^4$ is the rotation Quaternion and $\boldsymbol{v}_i \in \mathbb{R}^4$ is the translational Quaternion of the i^{th} continuum section relative to $\{O\}$.

A. Recursive Rotation and Translational Quaternions

From the definition given by (9), DQ of $(i-1)^{th}$ section is $\boldsymbol{Q}^{i-1} = \boldsymbol{u}_{i-1} + \epsilon \boldsymbol{v}_{i-1}$. Substituting this result into (9) yields

$$\boldsymbol{Q}^i = \boldsymbol{Q}_1 \odot \boldsymbol{Q}_2 \odot \cdots \odot \boldsymbol{Q}_i = \boldsymbol{Q}^{i-1} \odot \boldsymbol{Q}_i \tag{10}$$

If the DQ of i^{th} section DQ, i.e., $\boldsymbol{Q}_i = \boldsymbol{s}_i + \epsilon \boldsymbol{t}_i$ is substituted to (10), the rotational and translational components can be separately expanded as

$$\boldsymbol{u}_i\left(\xi_i, \boldsymbol{q}^i\right) = \boldsymbol{u}_{i-1}\left(\boldsymbol{q}^{i-1}\right) \circ \boldsymbol{s}_i\left(\xi_i, \boldsymbol{q}_i\right) \tag{11}$$

$$\begin{aligned}\boldsymbol{v}_i\left(\xi_i, \boldsymbol{q}^i\right) = \boldsymbol{v}_{i-1}\left(\boldsymbol{q}^{i-1}\right) \circ \boldsymbol{s}_i\left(\xi_i, \boldsymbol{q}_i\right) \\ + \boldsymbol{u}_{i-1}\left(\boldsymbol{q}^{i-1}\right) \circ \boldsymbol{t}_i\left(\xi_i, \boldsymbol{q}_i\right)\end{aligned} \tag{12}$$

Recursive DQ for any i^{th} section relative to $\{O\}$ is now completed. DQ velocity kinematics is presented next. Note that, for ease of notation, dependency variables are omitted from here onward.

B. Velocity Kinematics and Jacobians

Let $\mathbf{J}_i^u$ and $\mathbf{J}_i^v$ are respectively be the rotational and translation Quaternion Jacobians, defined as $\mathbf{J}_i^u = \nabla_{\boldsymbol{q}} \boldsymbol{u}_i \in \mathbb{R}^{4\times 3i}$ and $\mathbf{J}_i^v = \nabla_{\boldsymbol{q}} \boldsymbol{v}_i \in \mathbb{R}^{4\times 3i}$. Any j^{th} column of $\mathbf{J}_i^u$ is defined as $\left(\mathbf{J}_i^u\right)_j = \boldsymbol{u}_{i,j}$. Noting $\boldsymbol{q}^i = \left[\boldsymbol{q}^{i-1}, \boldsymbol{q}_i\right]$ thus $q_j \in \boldsymbol{q}^{i-1}$ or $q_j \in \boldsymbol{q}_i$, $\boldsymbol{q}^{i-1} \mapsto \mathbf{J}_i^u\left(\boldsymbol{q}^{i-1}\right)$, and from (11), $\left(\mathbf{J}_i^u\right)_j$ can be simplified to two separate cases as

$$\left(\mathbf{J}_i^u\right)_j = \begin{cases} \boldsymbol{u}_{i-1,j} \circ \boldsymbol{s}_i & ; q_j \in \boldsymbol{q}^{i-1} \\ \boldsymbol{u}_{i-1} \circ \boldsymbol{s}_{i,j} & ; q_j \in \boldsymbol{q}_i \end{cases} \tag{13}$$

From the definition of $\left(\mathbf{J}_i^u\right)_j$ it can be deduced that $\left(\mathbf{J}_{i-1}^u\right)_j = \boldsymbol{u}_{i-1,j}$. By substituting this result, now (13) can be simplified to

$$\left(\mathbf{J}_i^u\right)_j = \begin{cases} \left(\mathbf{J}_{i-1}^u\right)_j \circ \boldsymbol{s}_i & ; q_j \in \boldsymbol{q}^{i-1} \\ \boldsymbol{u}_{i-1} \circ \boldsymbol{s}_{i,j} & ; q_j \in \boldsymbol{q}_i \end{cases} \tag{14}$$

By similar reasoning and expression manipulation, the j^{th} column of the translational Jacobian can be derived. The recursive form of $\left(\mathbf{J}_i^v\right)_j$ is straightforward and is given by

$$\left(\mathbf{J}_i^v\right)_j = \begin{cases} \left(\mathbf{J}_{i-1}^v\right)_j \circ \boldsymbol{s}_i + \left(\mathbf{J}_{i-1}^u\right)_j \circ \boldsymbol{t}_i & ; q_j \in \boldsymbol{q}^{i-1} \\ \boldsymbol{v}_{i-1} \circ \boldsymbol{s}_{i,j} + \boldsymbol{u}_{i-1} \circ \boldsymbol{t}_{i,j} & ; q_j \in \boldsymbol{q}_i \end{cases} \tag{15}$$

The recursive relationship of the DQ Jacobians is now completed.

C. Deriving Cartesian Linear and Angular Velocities

The DQ Jacobians derived in (14) and (15) are however valid only in DQ space. In order to apply them in the Cartesian space, they must be transformed back into Cartesian velocities, i.e., linear and angular velocities about $\{O\}$.

The Cartesian angular velocity, $\Omega_i \in \mathbb{R}^3$ relative to $\{O\}$ can be recovered from Quaternion velocities as $\Omega_i = 2\dot{\boldsymbol{u}}_i \circ \boldsymbol{u}_i^*$ [23]. By definition, DQ kinematics make use of Quaternion products which involve cross products. However, computational operations for cross products are computationally slower with respect to matrix computations. The Quaternion product is a linear transformation of involved DQ's, hence there exists a matrix representation which can be readily derived by isolating relevant elements in matrix form. Thence, isolating velocity terms, it can be rearranged to

$\Omega_i = 2\,[\widetilde{\boldsymbol{u}}_i]\,\dot{\boldsymbol{u}}_i$ where $[\widetilde{\ }] \in \mathbb{R}^{3\times 4}$ defined in (16). Applying $\nabla_{\dot{\boldsymbol{q}}}$ to both sides and substituting Cartesian angular velocity Jacobian, $\mathbf{J}_i^{\Omega} = \nabla_{\dot{\boldsymbol{q}}}\Omega_i \in \mathbb{R}^{3\times 3i}$, and $\mathbf{J}_i^{u}$ listed in Section III-B, it is compactly rewritten as

$$\mathbf{J}_i^{\Omega} = 2\,[\widetilde{\boldsymbol{u}}_i]\,\mathbf{J}_i^{u} \tag{16}$$

where the matrix $[\widetilde{\boldsymbol{a}}]$ for Quaternion $\boldsymbol{a} = \langle a_1, a_2, a_3, a_0\rangle$ is defined as

$$[\widetilde{\boldsymbol{a}}] = \begin{bmatrix} a_0 & -a_3 & a_2 & -a_1 \\ a_3 & a_0 & -a_1 & -a_2 \\ -a_2 & a_1 & a_0 & -a_3 \end{bmatrix}.$$

Similarly, the position vector can be recovered from $\boldsymbol{v}_i$ of the DQ as $\boldsymbol{p} = 2\boldsymbol{v}_i \circ \boldsymbol{u}_i^*$ [23]. The linear velocity is recovered from the DQ component as $\boldsymbol{V}_i = 2\,[\bar{\boldsymbol{u}}_i]\,\dot{\boldsymbol{v}}_i - 2\,[\widetilde{\boldsymbol{v}}_i]\,\dot{\boldsymbol{u}}_i$. The Cartesian linear velocity Jacobian is defined as $\mathbf{J}_i^{V} = \nabla_{\dot{\boldsymbol{q}}}\boldsymbol{V}_i \in \mathbb{R}^{3\times 3i}$. The recursive velocity Jacobian is constructed as

$$\mathbf{J}_i^{V} = 2\,[\widetilde{\boldsymbol{u}}_i]\,\mathbf{J}_i^{v} - 2\,[\widetilde{\boldsymbol{v}}_i]\,\mathbf{J}_i^{u} \tag{17}$$

Note that, all Cartesian velocities are with reference to $\{O\}$.

IV. Comparison of Results

A. Prototype Arm,Validity of the Model, and Implementation

The mechanical parameters utilized herein were taken from the three-continuum section prototype arm shown in Fig. 1. Each continuum section is operated via three identical extending pneumatic muscle actuators having $L_{i0} = 0.15\,m$, $l_{min} = 0\,m$, and $l_{max} = 0.06\,m$ [24]. Rigid plastic mount frames of $r_i = 0.0125\,m$ were used to mount pneumatic muscle actuators and connect adjacent continuum sections with a $\frac{\pi}{3}$ rad angle offset about the Z' of $\{O_{i+1}\}$ (see Fig. 2). This offset helps mounting PMA's without crowding and enables routing pressure supply tubes.

The continuum arm kinematic model depend on the circular arc shaped deformation in individual continuum sections. However, continuum sections are subjected to external loading under the influence of gravity. These forces and moments can cause the deformation of continuum sections to deviate from the assumed circular arc shape. The evenly distributed constrainers (Fig. 6a) installed along the length of continuum sections significantly increase the elastic and torsional stiffness of the arm to mitigate possible deviations. Figure 6b compares a static pose of the prototype arm with the kinematic model given by (9). The respective pneumatic muscle actuator length changes of the prototype arm are substituted into the prototype arm kinematic model (see Fig. 6c). The curve parameters (λ_i and ϕ_i) of relevant continuum sections, computed utilizing the definitions given in [15], match and thus validate the circular arc assumption.

B. Multisection Arm Forward Kinematics

When multiple continuum sections are serially stacked together, the MSF errors of each section accumulate towards the arm tip. Therefore, the MSF order needs to be determined from the desired arm tip error. Figure 7a shows the arm tip position error variation for both modal HTM and modal

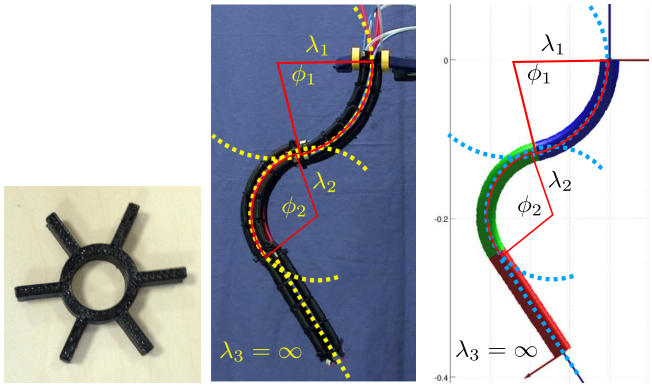

(a) (b) (c)

Fig. 6: Validating the circular arc assumption (a) Kinematic result comparison against the prototype continuum arm by overlaying the curvature radii of different sections: $\lambda_1 = 84.22$mm, $\phi_1 = 77.1°$,$\lambda_1 = 55.51$mm, $\phi_1 = 109.8°$, $\lambda_3 = \infty$, and $\phi_3 = 0$ where the values are computed according to [15]. Respective joint space variables are $\boldsymbol{q}_1 = [0.025,\ 0,\ 0]^T$, $\boldsymbol{q}_2 = [0,\ 0.036,\ 0]^T$, and $\boldsymbol{q}_3 = [0,\ 0,\ 0]^T$. (b) Direct kinematic result for the input joint space variables employed to generate Fig. 6b.

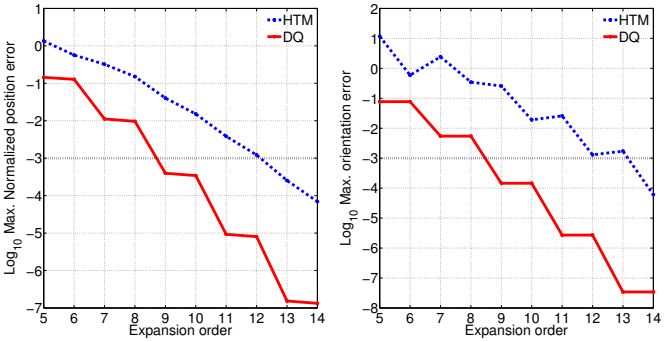

(a) (b)

Fig. 7: Three-section multisection continuum arm error comparison between the modal HTM and modal DQ method against the approximation expansion order (a) position error from (6) normalized to the original arm length, $3L_{i0} = 0.45m$, (b) maximum orientation error from (7). The reference lines denote 0.001.

DQ kinematics for the prototype arm. In this paper, an absolute (normalized to the unactuated length, $3L_0$, given within brackets) position error of 0.005m (~1%) at the three-section arm tip was considered acceptable. By referring to the plot, this requires 11^{th} order expansion for the modal HTM method but only 8^{th} order approximation was sufficient for the DQ approach. Further, according to Fig. 7b which shows the orientation error (computed from (7)), for the 8^{th} order approximation, modal DQ method produces about 10 times better orientation error performance.

This accuracy and numerical performance are also reflected in velocity kinematics. In order to quantitatively compare the error performance, the norm of matrix difference between the CP Jacobian and either DQ or modal HTM Jacobians are computed. First the CP linear and angular velocity Jacobians were recursively derived using (1) and its partial derivatives (see Appendix I). For the chosen MSF orders, the linear velocity Jacobian derived from both modal HTM and DQ methods yielded 0.736 and 0.038 errors (~20

times less). Similarly, the angular velocity Jacobian errors for modal HTM and DQ were 2.721 and 0.123 respectively (~22 times less). Also, the DQ method only consumed 66% computational time relative to the modal HTM method. These results confirm the accuracy and numerical efficiency of modal DQ based velocity kinematics.

C. Inverse Kinematics Trajectory Solutions

Next the performance for inverse position and inverse position with orientation are considered. First start and end points of a linear spatial trajectory are identified. Then 90 uniformly distributed linear position (and orientation in Section IV-C.2) trajectories are generated. Due to the high order polynomial nature of expressions and high redundancy, obtaining closed form inverse kinematics for the full task-space position and/or orientation for multisection continuum arms is computationally infeasible. Hence, iterative Newton-Raphson method employing the pseudo inverse, $\mathbf{J}^{\dagger} = \mathbf{J}^T \left(\mathbf{J}\mathbf{J}^T\right)^{-1}$, of linear velocity Jacobians $\left(\mathbf{J}^V \in \mathbb{R}^{3\times 9}\right)$ was used for inverse position solutions and Matlab's "`fmincon`" nonlinear optimization routine was employed for inverse orientation solutions. The choice of "`fmincon`" procedure was mainly due to the poor performance of iterative schemes for inverse orientation problems regardless of the HTM or DQ kinematics. This is because of the discontinuous nature of Euler angles in which case step error does not uniformly converge.

1) Inverse Position Kinematics: As a result of the numerical stability observed in the modal kinematics, higher solver gains are permitted in iterative calculations. Hence the algorithm rapidly converges to solutions (takes 5-9 iterations form random initial conditions) making the proposed modal approach suitable for computing IK solutions in real time (in the order of milliseconds). Because IK are solved in joint space this approach will incorporate joint variables within their mechanical ranges to ensure realizable solutions. Both modal HTM and DQ kinematics showed comparable performance in terms of number of iterations taken to reach the solution. However the DQ implementation consumed less computational time (~55%) for the task making it superior overall.

2) Inverse Orientation Kinematics: Accuracy and performance of modal HTM and modal DQ were compared for orientation IK for an illustrative trajectory. Figure 8 shows the instances of the trajectory following example for both modal HTM and modal DQ kinematics. The end points of the trajectory were [-0.1, -0.2, -0.35] and [0.1, -.02, -0.35] with orientation [π/2 0 0]. Matlab's "`fmincon`" with "`interior-point`" algorithm was used with absolute tolerance 0.005, 300 maximum iterations, and the error function $(0.1e_\alpha + e_p)$ where e_α is the ZYX Euler angle error and e_p is given in (6). The angle error was scaled to fit the position range. Both HTM and DQ methods consumed comparable times. However, the DQ kinematics were able to converge faster toward the solution for given constraints to produce a smooth and low-error trajectory in the joint-space (Fig. 8a). However the modal HTM kinematics convergence was slower hence the accuracy was poor

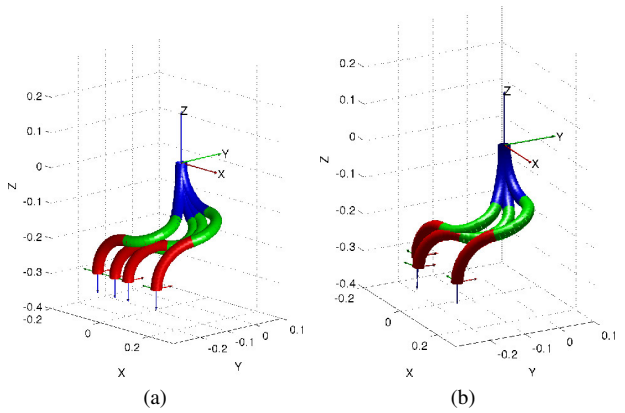

Fig. 8: Inverse orientation trajectory following snapshots. (a) DQ kinematics, (b) modal HTM kinematics. Note the smooth trajectory of DQ kinematics whereas modal HTM kinematics fails to reach solutions occasionally thus resulting non-smooth joint space trajectories.

with respect to modal DQ kinematics. Consequently the respective joint-space trajectory was not smooth and Fig. 8b shows one such instance where IK solution showing a relatively large error. Refer to the accompanying video for the visual simulation results of the inverse orientation kinematic trajectory following. This types of deviations are reflected on the joint space. In an actual situation, as a result of the high compliance, these cause large decaying oscillatory perturbations. Figure 9 compares the errors along the inverse trajectory points. The plot was generated by obtaining the mean error for 30 intermediate points solved for 30 times for better interpretation. The slow convergence and limited successful convergence of modal HTM is evident by observing the scattering of errors across the plot. Where as modal DQ solution range is significantly lower with high and more successful and consistent convergence to/closer-to solutions. Additionally, when the number of iterations was decreased keeping the error function constant at 0.005, not surprisingly, modal DQ method still maintained better error performance consuming less time than the modal HTM method. This has important implications for real-time inverse kinematic algorithm implementations. Finally, the the orientation $[0, \pi/2, 0]$ for the same trajectory given above is singular for modal HTM implementation hence failed to solve the trajectory but modal DQ kinematics produced the solution without any issues. Supplementary video includes the numerical results. Overall, the results conclude that modal DQ kinematics offer superior performance in both accuracy and computational time over both modal HTM and CP kinematics for multisection continuum arms.

V. Conclusions

In this paper, new modal DQ based kinematics were introduced for multisection continuum arms. The procedure for deriving the DQ representation from the CP kinematics and MSFs for DQ elements were detailed. These MSF's derived for a continuum section can be implemented functionally and used for continuum sections with different mechanical parameters. Recursive implementation of DQ Jacobians was

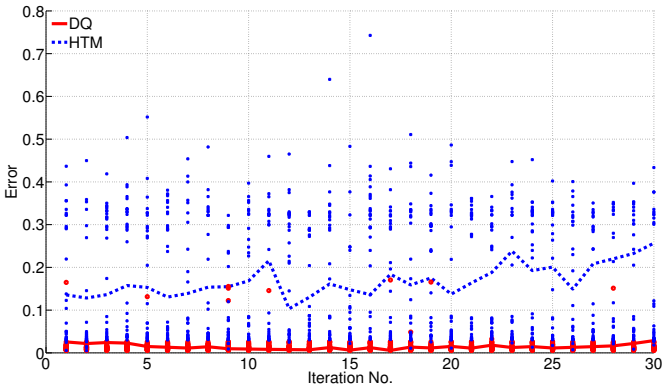

Fig. 9: Mean error comparison of inverse kinematic solutions between DQ and homogeneous transformation matrix kinematics for a 6-DoF spatial trajectory defined by 30 points. Note the small, consistent, and smooth error variation of DQ inverse kinematics.

presented. Illustrative numerical examples were then presented to compare the accuracy and computational efficiency of modal DQ against the modal HTM approach. Inverse position and orientation kinematics for spatial trajectory following examples showed the numerical stability of the modal DQ kinematics with efficient iterative numerical solutions for IK problems. The proposed modal DQ kinematics is easily extensible to variable length multisection continuum arm with more general actuator configurations and other serial rigid-linked robots.

REFERENCES

[1] W. McMahan, V. Chitrakaran, M. A. Csencsits, D. M. Dawson, I. D. Walker, B. A. Jones, M. B. Pritts, D. Dienno, M. Grissom, and C. D. Rahn, "Field trials and testing of the octarm continuum manipulator," in *IEEE Int. Conf. on Robotics and Automation*, 2006, pp. 2336–2341.

[2] H. Takanobu, T. Tandai, and H. Miura, "Multi-dof flexible robot base on tongue," in *IEEE Int. Conf. on Robotics and Automation*, 2004, pp. 2673–2678.

[3] I. D. Walker, D. M. Dawson, T. Flash, F. W. Grasso, R. T. Hanlon, B. Hochner, W. M. Kier, C. C. Pagano, C. D. Rahn, and Q. M. Zhang, "Continuum robot arms inspired by cephalopods," in *Procs. of the Int. Society for Optical Engineering*, 2005, pp. 303–314.

[4] I. S. Godage, D. T. Branson, E. Guglielmino, and D. G. Caldwell, "Path planning for multisection continuum arms," in *IEEE Int. Conf. on Mechatronics and Automation*, 2012, pp. 1208–1213.

[5] M. Hannan and I. Walker, "Analysis and initial experiments for a novel elephant's trunk robot," in *IEEE/RSJ Int. Conf. on Intelligent Robots and Systems*, pp. 330–337 vol.1.

[6] G. Robinson and J. B. C. Davies, "Continuum robots-a state of the art," in *IEEE Int. Conf. on Robotics and Automation*, 1999, pp. 2849–2854.

[7] I. S. Godage, D. T. Branson, E. Guglielmino, and D. G. Caldwell, "Pneumatic muscle actuated continuum arms: Modelling and experimental assessment," in *IEEE Int. Conf. on Robotics and Automation*, 2012, pp. 4980–4985.

[8] W. Rone and P. Ben-Tzvi, "Continuum robot dynamics utilizing the principle of virtual power," *IEEE Tran. on Robotics*, vol. 30, no. 1, pp. 275–287, Feb 2014.

[9] T. Zheng, I. S. Godage, D. T. Branson, R. Kang, E. Guglielmino, G. A. Medrano-Cerda, and D. G. Caldwell, "Octopus inspired walking robot: Design, control and experimental validation," in *IEEE Int. Conf. on Robotics and Automation*. IEEE, 2013, pp. 816–821.

[10] T. Zheng, D. T. Branson, R. Kang, M. Cianchetti, E. Guglielmino, M. Follador, G. A. Medrano-Cerda, I. S. Godage, and D. G. Caldwell, "Dynamic continuum arm model for use with underwater robotic manipulators inspired by octopus vulgaris," in *IEEE Int. Conf. on Robotics and Automation*, 2012, pp. 5289–5294.

[11] N. Giri and I. D. Walker, "Three module lumped element model of a continuum arm section," in *IEEE/RSJ Int. Conf. on Intelligent Robots and Systems*, 2011, pp. 4060–4065.

[12] T. Mahl, A. Hildebrandt, and O. Sawodny, "Forward kinematics of a compliant pneumatically actuated redundant manipulator," in *IEEE Conf. on Industrial Electronics and Applications*, 2012, pp. 1267–1273.

[13] G. S. Chirikjian and J. W. Burdick, "A modal approach to hyper-redundant manipulator kinematics," *IEEE Trans. on Robotics and Automation*, vol. 10, no. 3, pp. 343–354, Jun 1994.

[14] B. A. Jones and I. D. Walker, "Kinematics for multisection continuum robots," *IEEE Trans. on Robotics*, vol. 22, no. 1, pp. 43–55, 2006.

[15] I. S. Godage, E. Guglielmino, D. T. Branson, G. A. Medrano-Cerda, and D. G. Caldwell, "Novel modal approach for kinematics of multisection continuum arms," in *IEEE/RSJ Int. Conf. on Intelligent Robots and Systems*, 2011, pp. 1093–1098.

[16] J. Diebel, "Representing attitude: Euler angles, unit quaternions, and rotation vectors," *Matrix*, vol. 58, pp. 15–16, 2006.

[17] N. A. Aspragathos and J. K. Dimitros, "A comparative study of three methods for robot kinematics," *Systems, Man, and Cybernetics, Part B: Cybernetics, IEEE Transactions on*, vol. 28, no. 2, pp. 135–145, 1998.

[18] B. A. Jones and I. D. Walker, "Limiting-case analysis of continuum trunk kinematics," in *IEEE Int. Conf. on Robotics and Automation*, 2007, pp. 1363–1368.

[19] S. R. Buss, "Introduction to inverse kinematics with jacobian transpose, pseudoinverse and damped least squares methods," October 2004. [Online]. Available: http://math.ucsd.edu/~sbuss/ResearchWeb/ikmethods/iksurvey.pdf

[20] X. Wang and H. Zhu, "On the comparisons of unit dual quaternion and homogeneous transformation matrix," *Advances in Applied Clifford Algebras*, vol. 24, no. 1, pp. 213–229, 2014.

[21] I. S. Godage, G. A. Medrano-Cerda, D. T. Branson, E. Guglielmino, and D. G. Caldwell, "Modal kinematics for multisection continuum arms," *Bioinspiration & Biomimetics: Special Issue on Octopus-inspired robotics (Accepted for publication)*, 2014.

[22] J. Y. S. Luh, M. W. Walker, and R. P. C. Paul, "Resolved-acceleration control of mechanical manipulators," *IEEE Tran. on Automatic Control*, vol. 25, no. 3, pp. 468–474, Jun 1980.

[23] B. Graf, "Quaternions and dynamics," *arXiv preprint arXiv:0811.2889*, 2008.

[24] I. S. Godage, D. T. Branson, E. Guglielmino, G. A. Medrano-Cerda, and D. G. Caldwell, "Shape function-based kinematics and dynamics for variable length continuum robotic arms," in *IEEE Int. Conf. on Robotics and Automation*, 2011, pp. 452–457.

APPENDIX I
RECURSIVE HTM KINEMATICS

Recursive rotational and position matrices are given by

$$\Theta_i = \Theta_{i-1}\mathbf{R}_i \tag{I.1}$$

$$\Psi_i = \Psi_{i-1} + \Theta_{i-1}\boldsymbol{p}_i \tag{I.2}$$

The angular velocity vector and Jacobian with respect to $\{O\}$ is defined as $\omega = \left(\dot{\Theta}_i\Theta_i^T\right)^\vee$ and $\mathbf{J}_i^\Theta = \left(\nabla_{\boldsymbol{q}}\Theta_i\Theta_i^T\right)^\vee$ respectively. However for ease of implementation, we can define the angular velocity matrix such that $\Omega = \omega^\wedge = \nabla_{\boldsymbol{q}}\Theta_i\Theta_i^T$. Analogous to the DQ Jacobian derivation by considering $\boldsymbol{q}^i = \left[\boldsymbol{q}^{i-1}, \boldsymbol{q}_i\right]$ and substituting (I.1), $\left(\mathbf{J}_i^\Theta\right)_j = \left(\mathbf{J}_i^\omega\right)_j^\wedge$ is given by

$$\left(\mathbf{J}_i^\Theta\right)_j = \begin{cases} \left(\mathbf{J}_{i-1}^\Theta\right)_j & ;q_j \in \boldsymbol{q}^{i-1} \\ \Theta_{i-1}\mathbf{R}_{i,j}\mathbf{R}_i^T\Theta_{i-1}^T & ;q_j \in \boldsymbol{q}_i \end{cases} \tag{I.3}$$

Similarly, $\mathbf{J}_i^\Psi = \nabla_{\boldsymbol{q}}\Psi_i$ and the case-wise recursive $\left(\mathbf{J}_i^\Psi\right)_j$ is given by

$$\left(\mathbf{J}_i^\Psi\right)_j = \begin{cases} \left(\mathbf{J}_{i-1}^\Psi\right)_j + \left(\mathbf{J}_{i-1}^\Theta\right)_j\Theta_{i-1}\boldsymbol{p}_i & ;q_j \in \boldsymbol{q}^{i-1} \\ \Theta_{i-1}\boldsymbol{p}_{i,j} & ;q_j \in \boldsymbol{q}_i \end{cases} \tag{I.4}$$